FILLING OF CLOUD-INDUCED GAPS FOR LAND USE AND LAND COVER CLASSIFICATIONS AROUND REFUGEE CAMPS

Andreas Braun [(1)], Ron Hagensieker [(2)], Volker Hochschild [(3)]

[(1)] University of Tübingen, Rümelinstr. 19-23, 72072 Tübingen, Germany, Email: an.braun@uni-tuebingen.de
[(2)] Freie Universität Berlin, Malteserstr. 74 -100, 12249 Berlin, Germany, Email: ron.hagensieker@fu-berlin.de
[(3)] University of Tübingen, Rümelinstr. 19-23, 72072 Tübingen, Germany, Email: volker.hochschild@uni-tuebingen.de

ABSTRACT

Clouds cover is one of the main constraints in the field of optical remote sensing. Especially the use of multispectral imagery is affected by either fully obscured data or parts of the image which remain unusable. This study compares four algorithms for the filling of cloud induced gaps in classified land cover products based on Markov Random Fields (MRF), Random Forest (RF), Closest Spectral Fit (CSF) operators. They are tested on a classified image of Sentinel-2 where artificial clouds are filled by information derived from a scene of Sentinel-1. The approaches rely on different mathematical principles and therefore produced results varying in both pattern and quality. Overall accuracies for the filled areas range from 57 to 64 %. Best results are achieved by CSF, however some classes (e.g. sands and grassland) remain critical through all approaches.

1. BACKGROUND

Cloud-induced gaps in multispectral remote sensing imagery are a major constraint for the derivation of land cover products. According to the US Department of Energy about 52 % of global land surfaces are covered by clouds on average [1]. In addition, many regions of acute scientific interest, such as tropical forests, coastal areas, and urban sprawls tend to be especially affected by seasonal or full-year cloud coverage [2,3]. Therefore, handling cloud cover is of special interest in multispectral land cover mapping. Many approaches have been proposed to address this problem, including filtering, histogram matching, band substitution, or the use of complementary images of sensors which are not affected by atmospheric distortions [4-7].

The identification of land use and land cover (LULC) is one of the main tasks and challenges of remotely sensed images, especially when large areas are observed or when field-work is time consuming and expensive. Additionally, some areas are inaccessible due to terrain restrictions or threats to life or physical conditions. This applies to extreme climates, natural disasters or armed conflicts.

The United Nations High Commissioner for Refugees (UNHCR) estimated a total number of nearly 60 million people being forcibly displaced at the end of 2015 [8]. The main reasons are environmental changes at local, regional and global scales, poverty, social repression or prosecution as well violence through civil war or terrorism. These people often gather in refugee camps at random sites which were neither prepared nor suitable [9]. Relief agencies arriving at those camps after their establishment therefore struggle with the need for prompt action without any information about the site and the hosted population. Remote sensing can provide short-term information assisting the organization of the emergency response and the management of the camp [10]. But also long-term information has found to be helpful: The condition of the environment around the camp, the spatial distribution of resources such as drinking water or fire wood as well as their availability to the camp inhabitants and their development over several years [11].

While approaches to reduce effects of slight cirrus effects in images already exist [12,13] this paper focuses on the challenge of gaps in classified images induced by optically thick cloud patches in the context of provision of reliable LULC information in situations of emergency and humanitarian relief. These applications rely on mostly classified data or derived products rather than the raw multispectral imagery. However, waiting for a cloud free image can take several months in parts of the earth, especially in tropical and subtropical regions. Still delivering complete and reliable information is a key task for the observation of areas under humanitarian relief. We therefore test four different approaches which intend to restore missing information by smaller cloud patches in a classified scene based on ancillary information from synthetic aperture radar (SAR) data. Its independency from sunlight and its ability to penetrate cloud cover makes it a valuable source for image restoration. due to the fact that Sentinel-1A launched in 2013 by the European Space Agency (ESA) within the Copernicus program [14] is supported by a second satellite, Sentinel-1B, since April 2016 [15] images at dense time intervals are operationally provided for large parts of the earth, and thus reducing the temporal baseline between image acquisitions of optical and SAR sensors.

2. STUDY AREA & DATA

2.1. Study area

The study area lies in the Kurdistan Region in northern Iraq near the city of Dohuk which is located about 50 kilometers from the Syrian and Turkish border in the North and Northwest (Fig. 1). The region hosts a total number of nearly 50.000 refugees [16] distributed over two camps (Domiz 1 and Domiz 2) which have been opened in April 2012. Most of the inhabitants are from Kurdish regions of Syria fleeing from consequences of civil war.

The study area is characterized by extensive agricultural use, sparse vegetation cover (mainly limited to grassland, shrubs and mosses) and limestones formations and quaternary deposits [17]. The Tigris River reaches from Northwest to Southeast and discharges into the Mosul water reservoir in the center of the study area. the Mosul dam is Iraq's largest dam and was temporally captured by militia of the Islamic State during July and August 2014 who threatened to blow it up and flood the areas downstream, including the city of Mosul [18].

The climate is characterized by relatively high precipitation (average annual rainfall: 530 mm) with a rainy season from November and March, while there is little or no precipitation during the summer [17].

2.2. Data sets and preprocessing

For the sake of image congruence regarding phenology and land use a small temporal baseline between the optical and SAR image was needed. We therefore used a cloud-free scene of Sentinel-2 from 23 December 2015 and a SAR image of Sentinel-1 from 22 December 2015 in Interferometric Wide Swath (IW) in VV and VH polarization.

Sentinel-2 imagery was acquired as L2A products and radiometric calibration was applied in order to retrieve surface reflectance [19]. Lastly all 13 bands were resampled to a common spatial resolution of 10 meters.

Sentinel-1 imagery was acquired as a Level-1 SLC product at a spatial resolution of 10 meters. Pre-processing steps was performed as follows: Calibration to Beta Naught (β^0_{db}), TOPSAR Debursting [20], Terrain Correction to retrieve Terrain Flattened Gamma Naught (σ^0_{db}) [21] and projection to UTM zone 37N. No speckle removal was applied so that image texture is preserved. In order to increase the information inherent to the SAR image the following textures were calculated on both polarizations with kernel sizes of 7 and 11 pixels: Angular Second Moment, Contrast, Dissimilarity, Energy, Entropy, Correlation, Mean, Variance, High Pass, Low Pass, Maximum [22,23]. The resulting 105 rasters contained redundancies which were then reduced to 13 principal components via principal component analysis (PCA).

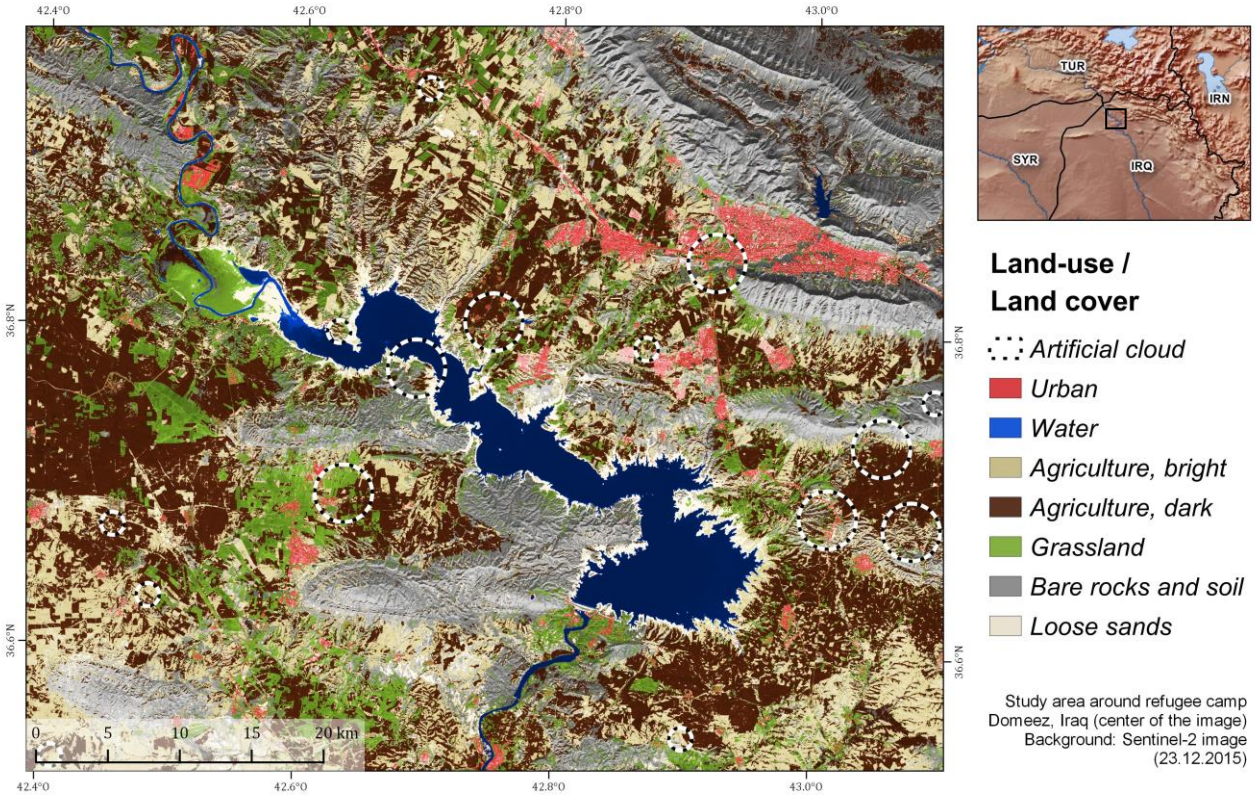

Figure 1: Location of the study area, main LULC classes and locations of the artificial clouds

3. METHODS

3.1. Initial classification

Classification was conducted using Import Vector Machine (IVM). IVM is a probabilistic classifier based on kernel logistic regression [22] which utilizes so-called import vectors as representatives for each class. With import vectors it is possible to reconstruct the distribution of each class, and class membership can hence be estimated. Therefore, opposed to conventional Support Vector Machine (SVM) classifiers, IVM generate a reliable probabilistic output natively [22]. Past studies show that IVM offer more conservative outputs than probabilistic SVM, and the probabilities can be considered more reliable in [23]. Moreover, due to their formulation IVM are inherently capable to address multi-class problems. Identical to standard SVM parameterization, we chose radial basis function (rbf) kernels, and parameterization of the IVM was conducted via grid search.

For this study we independently classified the Sentinel-2 and one Sentinel-1 scenes using 1900 manually collected and well distributed training samples. Note that classification from a probabilistic standpoint does not produce a grid carrying class labels, but one grid for each class, carrying the corresponding class probabilities at each location. Classification was then conducted via indexing the maximum at each location. Yet for further processing will be based on the probabilistic output. For an encompassing background on IVM and its applicability in remote sensing also see [24,25].

Twelve random points were generated with a radius of 750 or 2000 meters in order to imitate small patches of clouded areas. These areas were then cropped out and the information was considered lost.

3.2. Filling by Markov Random Fields

We formulated a grid-based Markov Random Field (MRF) to perform regularization on the probabilistic classification result [26]. The classification probabilities of each pixel can thus be understood as a node in the MRF, which is connected to its spatial neighbors (the adjacent pixels of the same image), and its temporal neighbors (the spatially congruent pixels of the corresponding S1/S2 scene). As is common practice [26], the probabilities were transferred into the energy space, and the total energy U of the classification respecting the Markov conditions is given by Eq. 1.

$$U(Y \mid X) = -\sum_{i \in I} \ln\left(p(y_i \mid x_i)\right) + \beta \sum_{i \sim j} 1 - \delta(y_i, y_j) \qquad (1)$$

Here pixel neighborhood (spatial as well as temporal), is defined by ~, and I describes the set of all classification probabilities to be addressed for the regularization procedure. δ serves as a function to promote heterogeneity, and is weighted using β.

Finding a classification to minimize the energy function (which is equivalent to the maximization of the probability), was achieved using a modified variant of Loopy Belief Propagation (LBP) [27]. LBP utilizes message passing to iteratively approach to a local minimum, which is considered a state with a high classification accuracy. For this, each node passes its "beliefs" on any potential class combination (C^2) to its neighbors, and evaluates the accordingly received messages using its individual bias, which is the energy as derived from the IVM classification. Repeated iteration of this passing procedure leads to messages being transported over the image, and eventual inference. While this method can be used for post classification regularization, its purpose in the context of this study is to pass messages from known areas into the cloud-induced gaps. Gaps are non-classified, and as such have uniformly distributed probabilities for each class. In contrast, areas surrounding the gaps (spatially as well as temporally), carry classification probabilities, and thus pass messages carrying these preferences into the masked out territory. As an experiment we formulated two different kinds of message passing framework: the mono-sensoral MRF utilizes just spatial messages, which are passed between the pixels of the Sentinel-2 classification image (MRF-S2), while the multi-sensoral MRF utilizes a neighboring Sentinel-1 scene to also pass messages in between spatially congruent pixels of both classification maps (MRF-S1+S2).

3.3. Filling by Random Forest

Random Forests (RF) detect patterns in training data by creating large numbers of different and uncorrelated classification and regression trees (CART [28]). In our case 1000 randomly distributed points outside the clouded areas were generated and trained by the underlying classes as well as the textural information of the SAR images. The RF then draws randomly selected subsets from the training data for the creation of classification rulesets [29]. In our case 500 independent trees were calculated and averaged to a final model. This model was then used to predict the missing class under clouded areas based on the SAR textures available (RF-S1). A training accuracy of 72.8 % was achieved.

3.4. Filling by Closest Spectral Fit

Closest Spectral Fit (CSF) [6] is a technique to reconstruct image information underneath clouded areas satellite images. This is achieved by comparing the information at each pixel with cloud cover in an auxiliary image (SAR data in our case) with its unclouded neighborhood. Based on its distance to the

clouded pixel a weighting is applied and the pixel with the smallest difference is identified. The image information is then transferred from this pixel into the corresponding clouded pixel in the original image thus progressively filling cloud pixels with the most probable information. This can be applied band-wise or, as in our case, to an already classified image. We generated one outcome per ancillary SAR image (see section 2.2) and took the majority of all results as a final result of the approach which then contained class information at the former cloud areas.

4. RESULTS & DISCUSSION

Each of the four approaches produced a classified map with restored information underneath the artificially generated clouds. A visual comparison is given in Fig. 2. It can be seen that the four approaches lead to different visual patterns according to the underlying principles. Visually, the MRF-S2 produced the least accurate results by only taking the distribution of classes at the edge of the clouds into account. RF-S1, MRF-S1+S2 and CSF-S1 performed similarly well although each approach has some weakness: As shown in test site A, all approaches are able to detect single buildings, however two of them are missing in RF-S1. Larger urban areas (test site C) were detected best in MRF-S1+S2 and are clearly overestimated by CSF-S1 and underestimated in RF-S1. Regarding water (test site B) all three approaches performed very good. This is due the low backscatter of water surfaces in SAR images.
Quantitative validation is based on manually collected sample areas under all twelve created clouds based on the original Sentinel-2 image thus ensuring that possible misclassifications in the original image are not taken into account for the creation of the confusion matrix.

The following accuracies are achieved:
MRF-S2: 59,98 %
MRF-S1+S2: 57,26 %
RF-S1: 60,19 %
CSF-S1: 64,82 %
Accordingly, CSF-S1 turns out to be the most efficient approach among the tested, followed by RF-S1.

Tab. 1 summarizes the user's and producer's accuracies (UA & PA) for the seven LULC classes underneath the clouds. As already indicated by the visual comparison, water achieves the highest accuracies throughout all approaches due to the sensitivity of the SAR backscatter towards its outstanding physical characteristics.
Dark agricultural areas are also of high accuracy, although their discrimination from light agricultural areas is hardly achieved by the SAR information alone. Urban areas show good user accuracies but are often overestimated in the results due to high SAR backscatter.
Most critical classes were loose sands and grassland due to their rarely distinctive features for the wavelengths of Sentinel-1's C-band.
RF-S1 produces good results but strongly relies on accurate reference information for the training of the classifier. CSF algorithm outperforms the other approaches in this study regarding overall accuracy, but has also problems with certain classes vanishing in the S1 image.

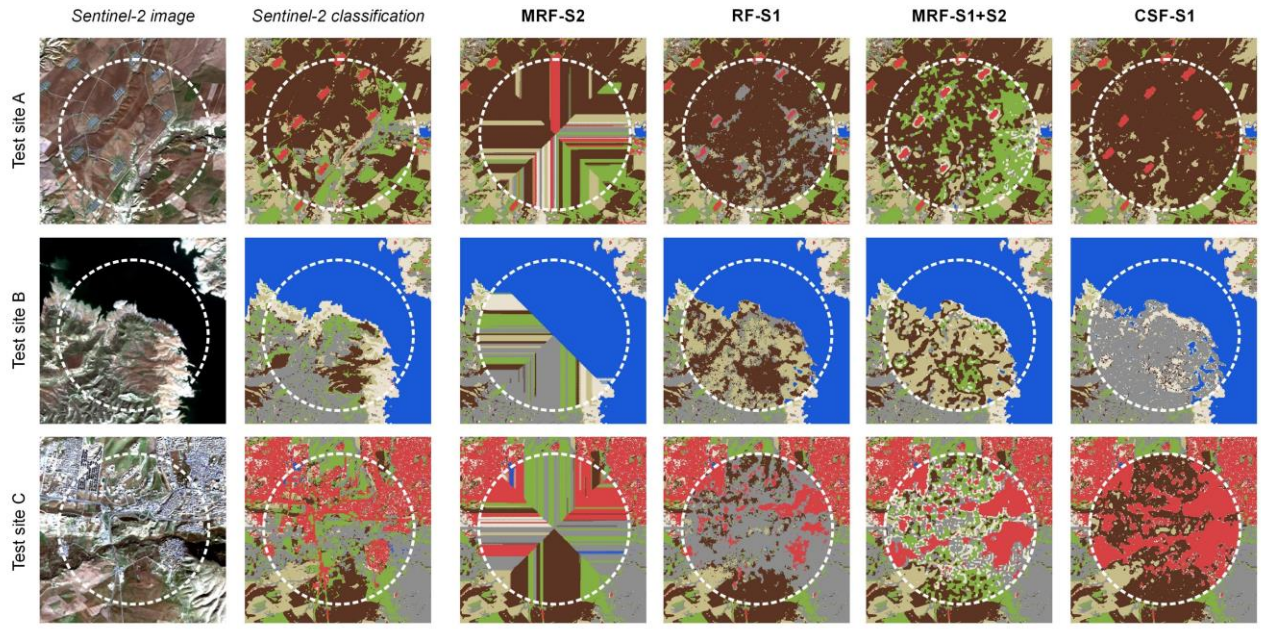

Figure 2: Visual comparison for three selected test sites.

Table 1: Accuracy assessment for the seven classes

	MRF-S1+S2		MRF-S2		RF-S1		CSF-S1	
	UA	PA	UA	PA	UA	PA	UA	PA
Urban	81,5 %	23,7 %	19,1 %	5,9 %	73,6 %	17,6 %	95,7 %	28,9 %
Water	96,1 %	99,3 %	78,9 %	95,3 %	97,1 %	99,3 %	93,1 %	98,5 %
Agriculture, light	48,6 %	61,1 %	45,2 %	61,2 %	49,3 %	53,5 %	58,6 %	66,8 %
Agriculture, dark	64,6 %	76,4 %	67,8 %	67,3 %	62,5 %	84,1 %	63,5 %	77,6 %
Grassland	10,7 %	8,4 %	48,9 %	38,7 %	39,1 %	10,4 %	66,9 %	25,7 %
Bare rocks and soil	53,0 %	24,8 %	57,1 %	83,4 %	30,0 %	55,0 %	37,9 %	70,0 %
Loose sands	17,4 %	13,1 %	48,7 %	20,8 %	40,2 %	6,7 %	74,8 %	29,0 %
Overall Accuracy	**57,26 %**		**59,98 %**		**60,19 %**		**64,82 %**	

It is notable and also quite ironical that MRF-S2 produces even slightly higher accuracies than MRF-S1+S2 which uses a classification of the neighboring Sentinel-1 scene as additional input and replicates homogeneous patches by systematically recognizing the context of each pixel. MRF-S2 is therefore highly dependent on the class distributions at the edges of clouds, thus producing unrealistic but very homogeneous patterns leading to partly correct classifications of larger areas such as water or bare rocks and soil. This explains the relatively high overall accuracy of 59.98 % of the purely probabilistic approach.

It can be argued that overall accuracies of all approaches are considerably low in terms of remote sensing. But it should be kept in mind that this study is not about image classification in the first place but tests how different methods perform when information is considered as completely lost. The question is if 65 % accuracy are better than zero information. In terms of multi-temporal monitoring of resources and gradual developments in land cover such numbers would be insufficient as the user could no longer be sure if changes are related to inaccuracies or to actual LULC change. The approach is rather suitable for simple reconstruction of missing areas to get a first and complete idea of the study area. All of the suggested approaches could as well be applied to Landsat ETM+ scenes acquired after 2003 when the scan-line corrector failed and images are characterized by gaps [30].

It turned out that performance of the approaches strongly depends on the number and selection of LULC classes. Some classes which can be clearly distinguished in the Sentinel-2 scene nearly remain invisible in the SAR image because they have similar backscatter characteristics as other classes. Reconstructing the spatial occurrence of those classes is nearly impossible with SAR data alone. MRF-S1+S2 provides a good alternative also considering class probabilities and spatial neighborhoods. In the end, large errors of commission and omission of few classes reduced the overall accuracy of each approach. One way to prevent this would be to perform the PCA on the SAR data before the initial classification of the optical scene and selecting suitable classes which can be identified in the PCA product.

Another point to discuss is the size of the clouds. While their proportion to the rest of the scene was comparably low in our case, larger cloud areas would cause problems for two of the approaches: MRF-S2 would lead to even more unrealistic patterns and RF-S1 would have fewer area to train the classifier on. This has to be taken into consideration when selecting one of the methods.

For future studies, each of the methods could be refined by taking into account spatial autocorrelation in the distribution of LULC classes [33]. Furthermore, a combination of several ancillary SAR images increase prediction accuracy. This could be achieved by using SAR images of different acquisition dates [34] or even different sensors to include the backscatter mechanisms at various wavelengths [7].

This paper showed how complete LULC information in situations of humanitarian relief can be provided if parts of the image are obscured by cloud cover. While many studies aim at the restoration of band information we focused on methods which can be automatically applied on already classified image within a short time and without further knowledge of a user. They can therefore be seen as examples for operational use.

ACKNOWLEDGEMENTS

This work was funded by the Austrian Research Promotion Agency (FFG) under the Austrian Space Applications Programme (ASAP 9/840081) and DLR/BMWi (FKZ 50 EE). Sentinel data was provided by Copernicus and the European Space Agency.

5. REFERENCES

1. Warren, S.G., Hahn, C.J., London, J., Chervin, R. & Jenne, R.L. (1986). Global distribution of total cloud cover and cloud type amounts over land. NCAR Tech. Note TN-273+STR. doi:10.5065/D6GH9FXB.

2. Ju, J. & Roy, D.P. (2008). The availability of cloud-free Landsat ETM+ data over the conterminous United States and globally. *Remote Sensing of Environment* 112(3), 1196–1211. doi:10.1016/j.rse.2007.08.011.

3. Asner, G.P. (2001). Cloud cover in Landsat observations of the Brazilian Amazon. *International Journal of Remote Sensing* 22(18), 3855–3862. doi:10.1080/01431160010006926.

4. Mitchell, O.R., Delp, B.J. & Chen, P.L. (1977). Filtering to remove cloud cover in satellite imagery. *IEEE Transactions on Geoscience Electronics* 15, 137–141. doi:10.1109/TGE.1977.6498971.

5. Saunders, R.W. (1986). An automated scheme for the removal of cloud contamination from AVHRR radiances over western Europe. *International Journal of Remote Sensing* 7(7), 867–886. doi:10.1080/01431168608948896.

6. Meng, Q., Borders, B.E., Cieszewski, C.J. & Madden, M. (2009). Closest Spectral Fit for Removing Clouds and Cloud Shadows. *Photogrammetric Engineering & Remote Sensing* 75(5), 569–576. doi:10.14358/PERS.75.5.569.

7. Eckardt, R., Berger C., Thiel, C. & Schmullius, C. (2013). Removal of Optically Thick Clouds from Multi-Spectral Satellite Images Using Multi-Frequency SAR Data. *Remote Sensing* 5(6), 2973–3006. doi:10.3390/rs5062973.

8. UNHR (2015). Mid-Year Trends 2015. Field Information and Coordination Support Section. Division of Programme Support and Management, Geneva.

9. UNHCR (2007). Handbook for Emergencies. The Emergency Preparedness and Response Section, Geneva.

10. Tiede, D., Füreder, P., Lang, S., Hölbling, D. & Zeil, P. (2013). Automated Analysis of Satellite Imagery to provide Information Products for Humanitarian Relief Operations in Refugee Camps. From Scientific Development towards Operational Services. *PFG Photogrammetrie, Fernerkundung, Geoinformation* 3, 185–195. doi:10.1127/1432-8364/2013/0169.

11. Lang, S., Füreder, P., Kranz, O., Card, B., Shadrock, R. & Papp, A. (2015). Humanitarian Emergencies: Causes, Traits, and Impacts as Observed by Remote Sensing. In Remote Sensing of Water Resources, Disasters, and Urban Studies (Ed. Thenkabail, P.), CRC Press, Taylor & Francis Group, London, UK. ISBN: 978-1-4822-1791-9, pp. 483–511.

12. Richter, R., Wang, X., Bachmann, M. & Schläpfer, D. (2011). Correction of cirrus effects in Sentinel-2 type of imagery. *International Journal of Remote Sensing* 32(10), 2931–2941.

13. Pflug, B., Makarau, A., & Richter, R. (2016). Processing Sentinel-2 data with ATCOR. *Geophysical Research Abstracts*. EGU General Assembly, 17-22 April 2016, Vienna, Austria.

13. Torres, R., Snoeij, P., Geudtner, D., Bibby, D., Davidson, M., Attema, E., Potin, P., Rommen, B., Floury, N., Brown, M., Navas Traver, I., Deghaye, Duesmann, P., Rosich, B., Miranda, N., Bruno, C., L'Abbate, M., Croci, R., Pietropaolo, A., Huchler, M. & Rostan, F. (2012). GMES Sentinel-1 mission. *Remote Sensing of Environment* 120, 9–24. doi:10.1016/j.rse.2011.05.028.

14. Potin, P., Miranda, N., Grimont, P., Bargellini, P., Monjoux, E., Martin, J., Desnos, Y., Roeder, J., Shurmer, I., O'Connel, A., Torres, R. & Krassenburg, M. (2015). Sentinel-1 mission status. *2015 IEEE International Geoscience and Remote Sensing Symposium (IGARSS)*, 2820–2823. doi:10.1109/IGARSS.2015.7326401

15. UNHCR (2015). Domiz 1 & 2 camp profile December 2015. Online at *http://data.unhcr.org/syrianrefugees/download.php?id=10626* (as of 15 May 2016).

16. Agha, M., Numan, N. & Ma'Äala, K. (1978). Field Guide for the Geology of the Duhok and Sinjar Areas. Fifth *Iraqi geological congress*, 28-31st December 1978, Baghdad.

17. Malas, N. (2015). Mosul Dam's Takeover by ISIS Raises Risk of Flooding. Constant Maintenance Needed to Avoid Catastrophic Failure of Dam's Structure. *The Wall Street Journal* 11 August 2015. Online at *http://www.wsj.com/articles/mosul-dams-takeover-by-isis-raises-risk-of-flooding-1407799954* (as of 15 May 2016).

18. Eklund, L. & Seaquist, J. (2015): Meteorological, agricultural and socioeconomic drought in the Duhok Governorate, Iraqi Kurdistan. *Natural Hazards* 7(1), 421–441. doi:10.1007/s11069-014-1504-x.

19. Main-Knorn, M., Pflug, B., Debaecker, V. & Louis, J. (2015). Calibration and validation plan for the L2A processor and products of the Sentinel-2 mission. *International Archives of the Photogrammetry, Remote Sensing and Spatial Information Sciences* XL-7(W3), 1249–1255, doi:10.5194/isprsarchives-XL-7-W3-1249-2015.

20. Veci, L., Lu, J., Prats-Iraola, P., Scheiber, R., Collard, F., Fomferra, N., & Engdahl, M. (2014). The Sentinel-1 Toolbox. *Proceedings of the IEEE International Geoscience and Remote Sensing Symposium (IGARSS)*, 1–3.

21. Small, D. (2011). Flattening Gamma: Radiometric Terrain Correction for SAR imagery. *Transaction on Geoscience and Remote Sensing* 48(8), 3081–3093. doi: 10.1109/TGRS.2011.2120616.

22. Haralick, R., Shanmugam, K., & Dinstein, I. (1973). Textural features for image classification. *IEEE Transactions on Systems, Man, and Cybernetics* 3(6), 610–621. doi:10.1109/TSMC.1973.4309314.

23. Liew, S. (1995). Texture analysis of SAR images. *Geoscience and Remote Sensing Symposium. IGARSS '95. 'Quantitative Remote Sensing for Science and Applications', International, Firenze.* 1412–1414. doi:10.1109/IGARSS.1995.521765.

24. Zhu, J. & Hastie, T. (2001). Kernel logistic regression and the import vector machine. *Advances in neural information processing systems*, 1081–108.

25. Roscher, R., Waske, B., & Förstner, W. (2012). Incremental import vector machines for classifying hyperspectral data. *IEEE Transactions on Geoscience and Remote Sensing* 50(9), 3463–3473. doi:10.1109/TGRS.2012.2184292.

26. Roscher, R., Förstner, W., & Waske, B. (2012). WITHDRAWN: I2VM: Incremental import vector machines. *Image and Vision Computing*, http://dx.doi.org/10.1016/j.imavis.2012.08.008. Online at *http://www.sciencedirect.com/science/article/pii/S0262885612001321* (as of 15 May 2016).

27. Roscher, R., Waske, B., & Förstner, W. (2010). Kernel Discriminative Random Fields for land cover classification. 2010 IAPR Workshop on Pattern Recognition in Remote Sensing (PRRS), 1–5. doi:10.1109/PRRS.2010.5742801.

28. Moser, G., Serpico, S. & Benediktsson, J. (2013). Land-cover mapping by Markov modeling of spatial-contextual information in very-high-resolution remote sensing images. *Proceedings of the IEEE* 101(3), 631–651. doi:10.1109/JPROC.2012.2211551.

29. Murphy, K., Weiss, Y., & Jordan, M. (1999): Loopy belief propagation for approximate inference: An empirical study. *Proceedings of the Fifteenth conference on Uncertainty in artificial intelligence*, 467–475.

30. Breiman, L., Friedman, J.H., Olshen, R.A. & Stone, C. (1984). *Classification and regression trees.* Belmont, Wadsworth, UK.

31. Breiman, L. (2001). Random Forests. *Machine Learning* 45(1), 5–32. doi:10.1023/A:1010933404324.

32. Markham, B. (2004). Landsat sensor performance: history and current status. *IEEE Transactions on Geoscience and Remote Sensing* 42(12), 2691–2694. doi: 10.1109/TGRS.2004.840720.

33. Vaccaro, R. (2000). Exploiting spatial correlation features for SAR image analysis. *IEEE Transactions on Geoscience and Remote Sensing* 38(3). 1212–1223. doi:10.1109/36.843013

34. Bruzzone, L. (2004). An advanced system for the automatic classification of multitemporal SAR images. *IEEE Transactions on Geoscience and Remote Sensing* 42(6), 1321–1334. doi:10.1109/TGRS.2004.826821.